International Journal of Non-Linear Mechanics 125 (2020) 103532

Contents lists available at ScienceDirect

International Journal of Non-Linear Mechanics

journal homepage: www.elsevier.com/locate/nlm

From continuous to snapping-back buckling: A post-buckling analysis for hyperelastic columns under axial compression

Yuzhen Chen, Lihua Jin *

Department of Mechanical and Aerospace Engineering, University of California, Los Angeles, CA 90095, USA

ARTICLE INFO

Keywords:
Buckling
Post-buckling
Snapping-back instability
Asymptotic analysis
Material and geometric nonlinearity

ABSTRACT

Since Euler's elastica, buckling of straight columns under axial compression has been studied for more than 260 years. A low width-to-length ratio column typically buckles at a critical compressive strain on the order of 1%, after which the compressive load continuously increases with the displacement. Here using a general continuum mechanics-based asymptotic post-buckling analysis in the framework of finite elasticity, we show that a straight hyperelastic column under axial compression exhibits complex buckling behavior. As its width-to-length ratio increases, the column can undergo transitions from continuous buckling, like the Euler buckling, to snapping-through buckling, and eventually to snapping-back buckling. The critical width-to-length ratios for the transitions of buckling modes are determined analytically. The effect of material compressibility on the buckling modes and their transitions is further investigated. Our study provides new insights into column buckling.

1. Introduction

Column buckling is traditionally viewed as a way of material failure. However, it has recently been harnessed to design functional mechanical metamaterials [1], in which column buckling lays the foundation of many advanced functionalities, such as tunable Poisson's ratios [2], programmable nonlinear responses [3], shape morphing [4–13], and multi-stability [14–16]. The behaviors of these metamaterials are strongly influenced by the buckling and post-buckling of columns.

The simplest description of column buckling is Euler's elastica, in which columns are modeled as linear elastic rods undergoing small deformation. This model predicts that a straight column subjected to a compressive force F or strain ε buckles at a critical condition F_{cr} or ε_{cr}, and that the post-buckling slope S defined in $\left(F - F_{cr}\right)/F_{cr} = S\left(\varepsilon - \varepsilon_{cr}\right)$ is a positive constant 1/2, independent of geometries and boundary conditions [17,18]. This excellently predicts the buckling behavior of slender columns. However, as columns become wide, their post-buckling behavior alters dramatically, since the critical strains for column buckling become large and thus both material and geometric nonlinearities start to play key roles in the post-buckling regimes. In our recent work [19], we showed that as the width-to-length ratio increases, the buckling mode of a straight hyperelastic column under axial compression switches from continuous, snapping-through, to snapping-back. Correspondingly, the initial post-buckling slope changes from positive to negative and eventually back to positive. To predict bending and buckling behaviors of wide columns, various beam models have been proposed to extend Euler's elastica [20–24]. However, no existing one-dimensional beam models can capture the transition between snapping-through and snapping-back modes with respect to the width-to-length ratio. The beam models in Refs. [20–22] consider axial and shear deformations but still keep the constitutive material linear. These beam models can predict that the initial post-buckling slope decreases from 1/2 as the width-to-length ratio increases, yet remains positive. A recent effort [24] was made to incorporate material nonlinearity while keep the beam extensible and shearable. The proposed beam model can capture that the initial post-buckling slope changes its sign from positive to negative as the width-to-length ratio increases, but never flips its sign back to positive if the width-to-length ratio further increases. This failure is because the high-order strain terms from geometric nonlinearity, which become non-trivial in the post-buckling regime of wide columns, are omitted in the model [19]. Moreover, the kinematic assumption [25] adopted in these beam models, where the cross sections of beams are assumed to remain plane and undistorted in the deformed configuration, no longer holds for wide columns.

Compared to one-dimensional beam models, a two-dimensional continuum mechanics-based bifurcation analysis, which takes into account both material and geometric nonlinearities, can accurately capture the buckling and post-buckling behavior of axially compressed columns. The onset of buckling for axially compressed columns has been thoroughly studied in the literature [26–31] by solving an incremental boundary value problem. To determine the post-buckling equilibrium paths and their stability, a general asymptotic technique is developed

* Corresponding author.
E-mail address: lihuajin@seas.ucla.edu (L. Jin).

https://doi.org/10.1016/j.ijnonlinmec.2020.103532
Received 26 April 2020; Received in revised form 5 June 2020; Accepted 11 June 2020
Available online 13 June 2020

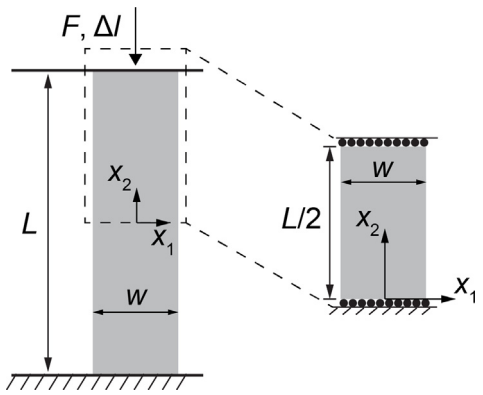

Fig. 1. Schematic representation of a two-dimensional hyperelastic column (left) subjected to a compressive force F or a displacement Δl. Due to symmetry, only the top half of this column (right) is selected for simulations and modeling.

by Koiter [17], and is widely utilized to find the post-buckling solutions for a compressed half-space of neo-Hokkean material [32], for a thin hyperelastic layer under compression [33], for a hyperelastic tube under axial compression [34], and for a growing elastic rod attached to an elastic foundation [35]. In particular, Ref. [36] addresses the post-buckling problem using this asymptotic method for a two-dimensional rectangular block with various constitutive laws, and finds that a stubby column under displacement-controlled compression can exhibit an unstable post-buckling equilibrium path, which corresponds to the snapping-back buckling mode. However, the whole spectrum of buckling modes for axially compressed columns with respect to the width-to-length ratio has not been analytically determined, which motivates our current work.

In this paper, we aim to analytically solve the initial post-buckling slope of a straight hyperelastic column under axial compression using a general asymptotic post-buckling analysis in the framework of finite elasticity, and capture the complete transitions of buckling modes from continuous, snapping-through, to snapping back with respect to the width-to-length ratio. Our results will be verified by finite element analysis (FEA). In Section 2, we expand our previous numerical findings to show that a two-dimensional hyperelastic column under axial compression can exhibit three different buckling modes as its width-to-length ratio varies. In Section 3, we conduct a continuum mechanics-based asymptotic analysis including both material and geometric nonlinearities in the model to determine the initial post-buckling slope as a function of the width-to-length ratio. Furthermore, the critical width-to-length ratios for the transitions of buckling modes are determined, and the effect of material compressibility on the critical values is investigated. The prediction on post-buckling response is in excellent agreement with finite element simulations. Conclusions are presented in Section 4.

2. Transition of buckling modes

We first conduct FEA using the commercial software Abaqus/Standard to identify the three buckling modes of a straight hyperelastic column under axial compression as the width-to-length ratio varies. The constitutive relation used in FEA is the compressible neo-Hookean material law with the following elastic energy density

$$W = \frac{\mu}{2}\left[J^{-2/3}\mathrm{tr}\left(\mathbf{F}\mathbf{F}^{\mathrm{T}}\right) - 2\right] + \frac{K}{2}(J-1)^2 \tag{1}$$

where $\mathbf{F}$ is the deformation gradient ($\mathrm{F}_{ij} = \partial u_i/\partial X_j + \delta_{ij}$, u_i denotes the displacement in X_i direction and δ_{ij} denotes the Kronecker delta), J is the determinant of $\mathbf{F}$, μ and K are the shear and bulk moduli, respectively. With the factor $J^{-2/3}$, the first term in the strain energy W in Eq. (1) is due to deviatoric deformation, while the second term is due to volumetric deformation. When K approaches infinity, the model represents an incompressible neo-Hookean material, which is adopted in the simulations in Fig. 2 to represent a generic hyperelastic material. We carry out two-dimensional plane strain simulations (Abaqus element type CPE8H) for columns with a width w and length L under an axial displacement Δl using the Riks method, and the compressive reaction force F is computed (Fig. 1). Both ends of the columns are allowed to slide freely along the horizontal direction but maintained flat. We assume reflection symmetry about the X_1 axis, and thus only half of this column is simulated. Imperfections are introduced into the initial geometry to trigger buckling and creasing instabilities (see Ref. [19] for further details).

We summarize the numerical results in Fig. 2 to show the three buckling modes for straight hyperelastic columns with different width-to-length ratios w/L under axial compression. We define the strain ε as $\Delta l/L$, which is the displacement Δl between the two ends of the column divided by the initial length L. We plot the normalized force–strain $F/w\mu$-ε curves along the equilibrium paths (the 2nd column of Fig. 2), and show the deformed shapes at three representative positions on the $F/w\mu$-ε curves: the onset of column buckling (Point 1, the 3rd column of Fig. 2), the onset of creasing [19,37–40], which is a scale-free, localized self-contacting fold, on the surface of the compressive side of the columns (Point 2, the 4th column of Fig. 2), and the rebound of the reaction forces (Point 3, the 5th column of Fig. 2). When w/L is low ($w/L = 0.10$, the 2nd row of Fig. 2), although the slope of the $F/w\mu$-ε curve decreases dramatically after buckling, it remains positive. We call this buckling mode as continuous buckling, since the post-buckling solution is stable, and the force and strain increase continuously. As w/L increases, the buckling behavior becomes discontinuous. When $w/L = 0.20$ (the 3rd row of Fig. 2), the force decreases while the strain increases after the buckling point (Point 1), leading to a negative initial post-buckling slope, which eventually increases sharply due to self-contact. This buckling mode with a negative initial post-buckling slope is called snapping-through buckling, which is commonly observed in shallow arches [41]. When $w/L = 0.28$ (the 4th row in Fig. 2), both the force and strain decrease after the buckling point (Point 1), forming a positive initial post-buckling slope. This buckling mode with such a force–strain relation resembles shell buckling [42], and is called snapping-back buckling. In sum, as w/L increases, the buckling mode undergoes a transition from continuous to snapping-through, and eventually to snapping-back. Correspondingly, the initial post-buckling slope switches from positive to negative, and ends up with positive.

Our previous numerical results [19] show that the critical w/L for the buckling mode transition from snapping-through to snapping-back for an incompressible neo-Hookean material is around 0.24, which has not been predicted by any existing beam model [20–24]. In the next section, we will analytically determine the initial post-buckling slope as a function of w/L and capture the transitions of buckling modes.

3. Continuum mechanics-based asymptotic analysis

In this section, we conduct a continuum mechanics-based asymptotic analysis [17,36,43] to investigate the buckling and post-buckling behavior of axially compressed columns. Ref. [36] has studied the stability of the post-buckling path of axially compressed columns. Here we further extend the analysis to determine the initial post-buckling slope, and investigate the transitions of buckling modes from continuous to snapping-back.

3.1. Bifurcation analysis

The potential energy for planar deformation of the half column shown in Fig. 1 is

$$\Pi[\mathbf{u};\varepsilon] = \int_A W\,dA = \int_0^{\frac{L}{2}}\int_{-\frac{w}{2}}^{\frac{w}{2}}\left\{\frac{\mu}{2}\left[J^{-2/3}\mathrm{tr}\left(\mathbf{F}\mathbf{F}^{\mathrm{T}}\right) - 2\right] + \frac{K}{2}(J-1)^2\right\}dX_1dX_2, \tag{2}$$

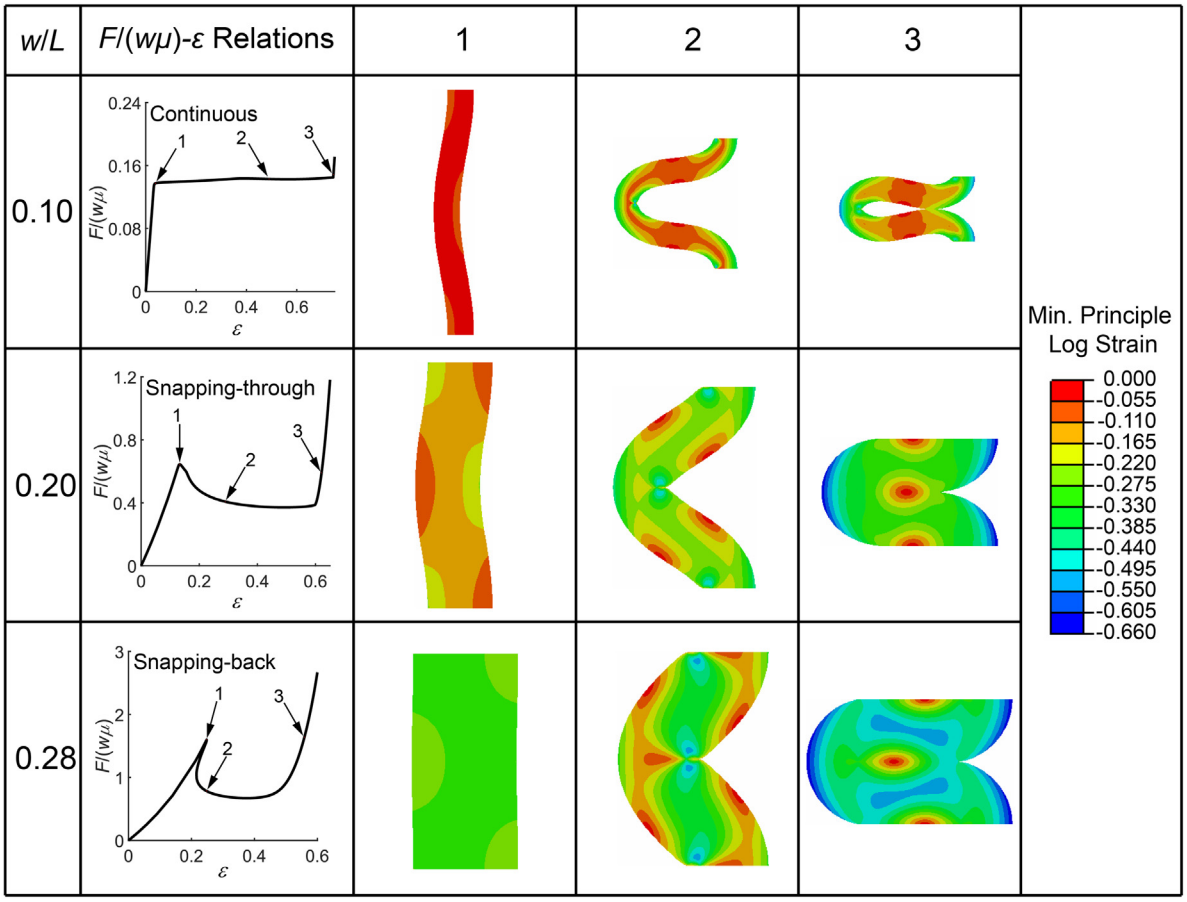

Fig. 2. Three modes of column buckling under axial compression: continuous (the 2nd row), snapping-through (the 3rd row), and snapping-back (the 4th row). The normalized compressive force $F/(w\mu)$ and strain ε relations are plotted in the 2nd column. The 3rd to 5th columns show how the shapes of the columns evolve as the compressive strain increases. The color indicates the level of minimum principle logarithmic strain. The shear-to-bulk modulus ratio μ/K adopted in FEA is 0, so that the material is perfectly incompressible. (For interpretation of the references to color in this figure legend, the reader is referred to the web version of this article.)

where $\mathbf{u}$ denotes the displacement field, W is the elastic energy density function given by Eq. (1). The variational equation of equilibrium can be obtained by applying the principle of stationary potential energy, i.e.

$$\Pi'[\mathbf{u};\varepsilon]\,\delta\mathbf{u} = 0, \tag{3}$$

where Π' denotes the first-order functional derivative of Π with respect to $\mathbf{u}$.

There exists a fundamental solution to Eq. (3), which is denoted as $\overset{0}{\mathbf{u}}$. This solution corresponds to homogeneous deformation and can be expressed in terms of the principle stretches

$$\overset{0}{\mathbf{u}} = \begin{bmatrix} \overset{0}{u}_1 \\ \overset{0}{u}_2 \end{bmatrix} = \begin{bmatrix} (\lambda_1 - 1)\,X_1 \\ (\lambda_2 - 1)\,X_2 \end{bmatrix}, \tag{4}$$

where λ_1 and λ_2 are the two principle stretches in the X_1 and X_2 directions, and can be determined by

$$\frac{\partial W}{\partial \lambda_1} = 0, \lambda_2 = 1 - \varepsilon. \tag{5}$$

The first equation in Eq. (5) indicates that the first Piola–Kirchhoff stress vanishes in the X_1 direction.

The fundamental solution $\overset{0}{\mathbf{u}}$ in Eq. (4) is stable until ε reaches $\varepsilon_{\mathrm{cr}}$, where another solution to Eq. (3) corresponding to column buckling emerges. The critical strain $\varepsilon_{\mathrm{cr}}$ for column buckling can be analytically determined by solving the following eigenvalue problem [17,36,43]

$$\Pi''\left[\overset{0}{\mathbf{u}}\left(\varepsilon_{\mathrm{cr}}\right);\varepsilon_{\mathrm{cr}}\right]\overset{1}{\mathbf{u}}\delta\mathbf{u} = 0 \tag{6}$$

for all admissible displacement fields $\delta\mathbf{u}$, where Π'' is the second-order functional derivative of Π with respect to $\mathbf{u}$, $\overset{0}{\mathbf{u}}\left(\varepsilon_{\mathrm{cr}}\right)$ is the fundamental solution at $\varepsilon_{\mathrm{cr}}$, and $\overset{1}{\mathbf{u}}$ is the buckling mode.

Substituting Eq. (2) into Eq. (6), we have

$$\Pi''\left[\overset{0}{\mathbf{u}}\left(\varepsilon_{\mathrm{cr}}\right);\varepsilon_{\mathrm{cr}}\right]\overset{1}{\mathbf{u}}\delta\mathbf{u} = \int_0^{\frac{L}{2}}\int_{-\frac{w}{2}}^{\frac{w}{2}} \frac{\partial^2 W\left[\overset{0}{\mathbf{u}}\left(\varepsilon_{\mathrm{cr}}\right)\right]}{\partial u_{k,l}\partial u_{i,j}}\overset{1}{u}_{i,j}\delta u_{k,l}\,dX_1\,dX_2 = 0, \tag{7}$$

where u_i and $\overset{1}{u}_i$ are the components of $\mathbf{u}$ and $\overset{1}{\mathbf{u}}$ in the X_i direction, respectively, and $()_{,j}$ equals $\partial()/\partial X_j$. Integration by parts yields the Euler–Lagrange differential equations for $\overset{1}{\mathbf{u}}$

$$\frac{\partial^2 W\left[\overset{0}{\mathbf{u}}\left(\varepsilon_{\mathrm{cr}}\right)\right]}{\partial u_{k,l}\partial u_{i,j}}\overset{1}{u}_{i,jl} = 0, \tag{8}$$

and the corresponding boundary conditions

$$\frac{\partial^2 W\left[\overset{0}{\mathbf{u}}\left(\varepsilon_{\mathrm{cr}}\right)\right]}{\partial u_{k,1}\partial u_{i,j}}\overset{1}{u}_{i,j} = 0 \text{ at } X_1 = \pm\frac{w}{2}, \tag{9}$$

$$\delta u_2 = 0 \text{ and } \frac{\partial^2 W\left[\overset{0}{\mathbf{u}}\left(\varepsilon_{\mathrm{cr}}\right)\right]}{\partial u_{1,2}\partial u_{i,j}}\overset{1}{u}_{i,j} = 0 \text{ at } X_2 = 0 \text{ and } L/2, \tag{10}$$

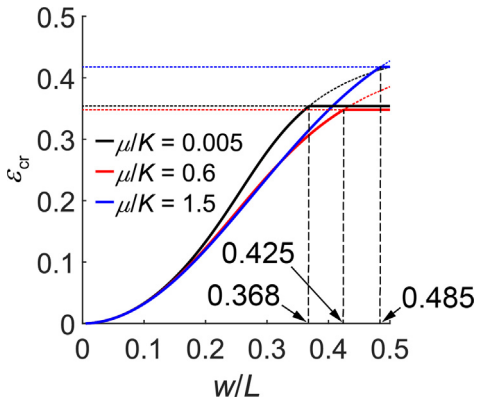

Fig. 3. Critical strain ε_{cr} for the onset of column instability as a function of the width-to-length ratio w/L under different shear-to-bulk modulus ratios μ/K. The curves represent the critical strain for column buckling, while the horizontal dotted lines indicate the critical strain for creasing in a homogeneously compressed slab. They intersect at a critical w/L, below which buckling occurs first and above which creasing occurs first.. (For interpretation of the references to color in this figure legend, the reader is referred to the web version of this article.)

where $()_{,jl}$ equals $\partial^2()/\partial X_j \partial X_l$. Eq. (10) holds automatically. The solutions to Eq. (8) can be written in the following form

$$\begin{cases} \overset{1}{u}_1 = \left(\alpha_1 \cosh z_1 X_1 + \alpha_2 \cosh z_2 X_1\right) \cos \frac{2\pi X_2}{L} \\ \overset{1}{u}_2 = \left(\alpha_3 \sinh z_1 X_1 + \alpha_4 \sinh z_2 X_1\right) \sin \frac{2\pi X_2}{L}, \end{cases} \tag{11}$$

where z_1 and z_2 are the two positive roots of the characteristic polynomial for Eq. (8). Substituting Eq. (11) into Eqs. (8) and (9), we then obtain

$$\mathbf{A} \begin{bmatrix} \alpha_1 \\ \alpha_2 \\ \alpha_3 \\ \alpha_4 \end{bmatrix} = 0. \tag{12}$$

A nontrivial solution to Eq. (12) exists when the determinant of the coefficient matrix $\mathbf{A}$ vanishes, from which we can solve ε_{cr}. With Eq. (12) and

$$\langle \overset{1}{\mathbf{u}}, \overset{1}{\mathbf{u}} \rangle = \frac{2}{Lw} \int_0^{\frac{L}{2}} \int_{-\frac{w}{2}}^{\frac{w}{2}} \overset{1}{u}_i \overset{1}{u}_i dX_1 dX_2 = 1, \tag{13}$$

we can determine the coefficients $\alpha_1 \sim \alpha_4$ that lead to the buckling mode $\overset{1}{\mathbf{u}}$ with a unit amplitude.

The critical strain for the onset of column buckling ε_{cr} depends on the shear-to-bulk modulus ratio μ/K and width-to-length ratio w/L. Fig. 3 plots ε_{cr} for column buckling as a function of w/L under three different μ/K. Under a given μ/K, the critical strain ε_{cr} increases monotonically from zero with the increase of w/L. Similar results have been reported in Ref. [36]. However, the dependence of ε_{cr} on μ/K is non-monotonic. For thick columns, $w/L > 0.35$, the case with an intermediate μ/K (the red curve in Fig. 3) has the lowest ε_{cr}. Once the critical strain for the onset of buckling surpasses that of creasing for sufficiently a high w/L, creasing occurs prior to buckling at a constant critical strain ε_{cr} (horizontal dotted lines) [19,39,40]. The critical strain for the onset of creasing under a plane strain condition is 0.354 for incompressible neo-Hookean material ($\mu/K = 0$) [39,40] and varies non-monotonically as μ/K increases [44]. The intersection between the critical conditions of buckling and creasing determines the critical w/L, below which buckling occurs first and above which creasing occurs first.

3.2. Post-buckling analysis

Having determined the critical strain ε_{cr} for the onset of buckling and the corresponding eigenmode $\overset{1}{\mathbf{u}}$, we asymptotically expand [17,36,43] the displacement field $\mathbf{u}$ and compressive strain ε in the vicinity of the buckling point along the equilibrium path of column buckling

$$\mathbf{u} = \overset{0}{\mathbf{u}}(\varepsilon) + \xi \overset{1}{\mathbf{u}} + \xi^2 \overset{2}{\mathbf{u}} + o\left(\xi^3\right), \tag{14}$$

$$\varepsilon = \varepsilon_{cr} + \xi^2 \varepsilon_2 + o\left(\xi^4\right), \tag{15}$$

where ξ represents the amplitude of the buckling mode $\overset{1}{\mathbf{u}}$. Due to symmetry, only even power terms of ξ are involved in Eq. (15) so that the sign of ξ has no effect on ε. Since $\mathbf{u}$ and ε given by Eqs. (14) and (15) must satisfy equilibrium $\Pi'[\mathbf{u};\varepsilon]\delta\mathbf{u} = 0$, a Taylor-series expansion about the buckling point gives

$$\left(\Pi''_{cr} \overset{2}{\mathbf{u}} + \frac{1}{2}\Pi'''_{cr} \overset{1}{\mathbf{u}}^2\right)\delta\mathbf{u}\xi^2 + \left(\varepsilon_2 \dot{\Pi}''_{cr} \overset{1}{\mathbf{u}} + \Pi'''_{cr} \overset{1}{\mathbf{u}} \overset{2}{\mathbf{u}} + \frac{1}{6}\Pi^{(iv)}_{cr} \overset{1}{\mathbf{u}}^3\right)\delta\mathbf{u}\xi^3 + o\left(\xi^4\right) = 0, \tag{16}$$

where $\Pi^{(n)}_{cr}$ is the nth-order functional derivative of Π at the buckling point, i.e. $\Pi^{(n)}\left[\overset{0}{\mathbf{u}}(\varepsilon_{cr}); \varepsilon_{cr}\right]$, and $\dot{()}$ is the first derivative with respect to ε. The coefficients of ξ^2 and ξ^3 in Eq. (16) must vanish independently, which yields a variational equation for $\overset{2}{\mathbf{u}}$

$$\Pi''_{cr} \overset{2}{\mathbf{u}}\delta\mathbf{u} + \frac{1}{2}\Pi'''_{cr}\left(\overset{1}{\mathbf{u}}\right)^2 \delta\mathbf{u} = 0, \tag{17}$$

and an expression for ε_2 by setting $\delta\mathbf{u} = \overset{1}{\mathbf{u}}$

$$\varepsilon_2 = -\frac{\Pi'''_{cr}\left(\overset{1}{\mathbf{u}}\right)^2 \overset{2}{\mathbf{u}} + \frac{1}{6}\Pi^{(iv)}_{cr}\left(\overset{1}{\mathbf{u}}\right)^4}{\dot{\Pi}''_{cr}\left(\overset{1}{\mathbf{u}}\right)^2}. \tag{18}$$

Substituting Eq. (2) into Eq. (17), we have

$$\int_0^{\frac{L}{2}} \int_{-\frac{w}{2}}^{\frac{w}{2}} \left[\frac{\partial^2 W\left[\overset{0}{\mathbf{u}}(\varepsilon_{cr})\right]}{\partial u_{i,j}\partial u_{k,l}} \overset{2}{u}_{k,l} + \frac{1}{2}\frac{\partial^3 W\left[\overset{0}{\mathbf{u}}(\varepsilon_{cr})\right]}{\partial u_{i,j}\partial u_{m,n}\partial u_{k,l}} \overset{1}{u}_{k,l} \overset{1}{u}_{m,n}\right]\delta u_{i,j} dX_1 dX_2 = 0. \tag{19}$$

Integration by parts yields Euler–Lagrange differential equations for $\overset{2}{\mathbf{u}}$

$$\frac{\partial^2 W\left[\overset{0}{\mathbf{u}}(\varepsilon_{cr})\right]}{\partial u_{i,j}\partial u_{k,l}} \overset{2}{u}_{k,lj} + \frac{1}{2}\frac{\partial^3 W\left[\overset{0}{\mathbf{u}}(\varepsilon_{cr})\right]}{\partial u_{i,j}\partial u_{m,n}\partial u_{k,l}}\left(\overset{1}{u}_{k,lj} \overset{1}{u}_{m,n} + \overset{1}{u}_{k,l} \overset{1}{u}_{m,nj}\right) = 0, \tag{20}$$

and the corresponding boundary conditions

$$\frac{\partial^2 W\left[\overset{0}{\mathbf{u}}(\varepsilon_{cr})\right]}{\partial u_{i,1}\partial u_{k,l}} \overset{2}{u}_{k,l} + \frac{1}{2}\frac{\partial^3 W\left[\overset{0}{\mathbf{u}}(\varepsilon_{cr})\right]}{\partial u_{i,1}\partial u_{m,n}\partial u_{k,l}} \overset{1}{u}_{k,l} \overset{1}{u}_{m,n} = 0 \text{ at } X_1 = \pm\frac{w}{2}, \tag{21}$$

$$\delta u_2 = 0 \text{ and } \frac{\partial^2 W\left[\overset{0}{\mathbf{u}}(\varepsilon_{cr})\right]}{\partial u_{1,2}\partial u_{k,l}} \overset{2}{u}_{k,l} + \frac{1}{2}\frac{\partial^3 W\left[\overset{0}{\mathbf{u}}(\varepsilon_{cr})\right]}{\partial u_{1,2}\partial u_{m,n}\partial u_{k,l}} \overset{1}{u}_{k,l} \overset{1}{u}_{m,n} = 0 \text{ at } X_2 = 0 \text{ and } L/2. \tag{22}$$

Eq. (22) is satisfied automatically. With the orthogonality between $\overset{1}{\mathbf{u}}$ and $\overset{2}{\mathbf{u}}$

$$\langle \overset{1}{\mathbf{u}}, \overset{2}{\mathbf{u}} \rangle = \frac{2}{Lw} \int_0^{\frac{L}{2}} \int_{-\frac{w}{2}}^{\frac{w}{2}} \overset{1}{u}_i \overset{2}{u}_i dX_1 dX_2 = 0, \tag{23}$$

the solutions to Eq. (20) can be written in the following form

$$\begin{cases} \overset{2}{u}_1 = B_1\left(X_1\right) \cos \frac{4\pi X_2}{L} + C_1\left(X_1\right) \\ \overset{2}{u}_2 = B_2\left(X_1\right) \sin \frac{4\pi X_2}{L}. \end{cases} \tag{24}$$

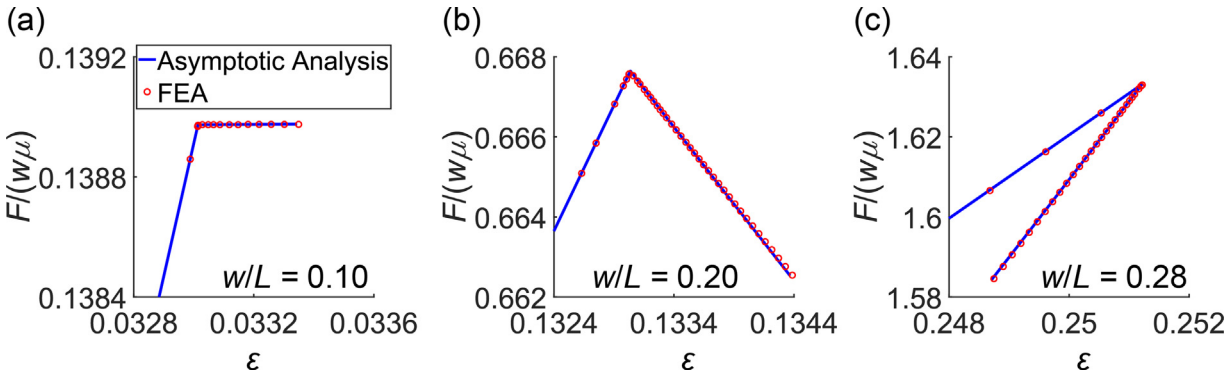

Fig. 4. Comparison between the post-buckling paths predicted by the asymptotic analysis (the solid lines) and FEA (the dots) under $\mu/K = 0.005$ for the three column buckling modes: (a) continuous ($w/L = 0.10$), (b) snapping-through ($w/L = 0.20$), and (c) snapping-back ($w/L = 0.28$).

$$\varepsilon_2 = -\frac{\int_0^{\frac{L}{2}}\int_{-\frac{w}{2}}^{\frac{w}{2}} \frac{\partial^3 W\left[\overset{0}{\mathbf{u}}(\varepsilon_{\mathrm{cr}})\right]}{\partial u_{i,j}\partial u_{k,l}\partial u_{m,n}} \overset{1}{u}_{m,n}\overset{1}{u}_{k,l}\overset{2}{u}_{i,j}\,dX_1dX_2 + \frac{1}{6}\int_0^{\frac{L}{2}}\int_{-\frac{w}{2}}^{\frac{w}{2}} \frac{\partial^4 W\left[\overset{0}{\mathbf{u}}(\varepsilon_{\mathrm{cr}})\right]}{\partial u_{i,j}\partial u_{k,l}\partial u_{m,n}\partial u_{p,q}} \overset{1}{u}_{p,q}\overset{1}{u}_{m,n}\overset{1}{u}_{k,l}\overset{1}{u}_{i,j}\,dX_1dX_2}{\int_0^{\frac{L}{2}}\int_{-\frac{w}{2}}^{\frac{w}{2}} \frac{d}{d\varepsilon}\left(\frac{\partial^2 W\left[\overset{0}{\mathbf{u}}(\varepsilon)\right]}{\partial u_{i,j}\partial u_{k,l}}\right)\Big|_{\varepsilon=\varepsilon_{\mathrm{cr}}} \overset{1}{u}_{k,l}\overset{1}{u}_{i,j}\,dX_1dX_2}. \tag{25}$$

Box I.

Substituting Eq. (24) into Eqs. (20) and (21), we can obtain $\overset{2}{\mathbf{u}}$. Then ε_2 can be calculated by substituting $\overset{2}{\mathbf{u}}$ and Eq. (2) into Eq. (18) we get Eq. (25) of Box I.

Given a specified compressive strain ε, we can obtain the displacement field $\mathbf{u}$ on the equilibrium path of column buckling using Eqs. (14) and (15). The applied force F corresponding to ε can then be calculated by

$$F = -\int_{-\frac{w}{2}}^{\frac{w}{2}} \frac{\partial W}{\partial u_{1,1}}\bigg|_{X_2=L/2} dX_1 = F_{\mathrm{cr}} + \xi^2 F_2 + o\left(\xi^4\right), \tag{26}$$

where F_{cr} is the critical force for column buckling. Combining Eqs. (15) and (26) and eliminating the intermediate variable ξ^2, we can write the relation between force F and strain ε in the following form

$$\left(F - F_{\mathrm{cr}}\right)/F_{\mathrm{cr}} = S\left(\varepsilon - \varepsilon_{\mathrm{cr}}\right) + o\left[\left(\varepsilon - \varepsilon_{\mathrm{cr}}\right)^2\right], \tag{27}$$

where S is the post-buckling slope in the vicinity of the buckling point

$$S = \frac{F_2}{\varepsilon_2 F_{\mathrm{cr}}}. \tag{28}$$

To verify this post-buckling analysis, we compare the post-buckling paths predicted by Eq. (27) with FEA under $\mu/K = 0.005$ (nearly incompressible neo-Hookean materials) (Fig. 4). We select three values of w/L representing the three column buckling modes: $w/L = 0.10$ (continuous), $w/L = 0.20$ (snapping-through), and $w/L = 0.30$ (snapping-back). In each case, the strain ε in the post-buckling regime is restricted to 1% higher (continuous and snapping-through) or lower (snapping-back) than the corresponding critical strain $\varepsilon_{\mathrm{cr}}$ such that Eq. (27) with only linear order term of $\left(\varepsilon - \varepsilon_{\mathrm{cr}}\right)$ can provide an accurate approximation of the force F. The post-buckling slope S defined in Eq. (27) for different w/L can be calculated using Eq. (28), yielding 0.02974 for $w/L = 0.10$, −5.788 for $w/L = 0.20$ and 12.06 for $w/L = 0.28$. As a result, the post-buckling paths predicted by Eq. (27) (the blue solid lines) and by FEA (the red circles) are in excellent agreement (percent error < 0.02%) (Fig. 4). Even if the strain ε in the post-buckling regime increases (continuous and snapping-through) or decreases (snapping-back) from the critical strain $\varepsilon_{\mathrm{cr}}$ by 5%, the predictions made by Eq. (27) on the post-buckling paths are still reasonably accurate (percent error < 0.3%).

We further compare the buckled shapes predicted by the asymptotic analysis and FEA when the strain ε in the post-buckling regime reaches $1.05\varepsilon_{\mathrm{cr}}$ (continuous and snapping-through) or $0.95\varepsilon_{\mathrm{cr}}$ (snapping-back) (Fig. 5). The buckled shapes predicted by our theory are in good agreement with FEA for all the three buckling modes. Note that when w/L is large, especially for the snapping-back case, the columns undergo large shear deformation, as assumed in the Timoshenko beam theory [20–22,25] Moreover, the initially flat cross sections do not remain flat after buckling, which is violated in the Timoshenko's assumption and the other existing beam models adopting the Timoshenko's assumption [20–24].

To study how the initial post-buckling slope S varies with w/L, we first investigate the two factors determining S in Eq. (28), F_2 and ε_2. We plot the normalized F_2/F_{cr} (Fig. 6a) and $\varepsilon_2/\varepsilon_{\mathrm{cr}}$ (Fig. 6b) as a function of w/L under different μ/K, and find that both F_2 and ε_2 monotonically decrease with w/L from a positive value and pass zero at certain w/L. The condition $F_2 = 0$ given a positive ε_2 indicates that S changes its sign from positive to negative, whereas $\varepsilon_2 = 0$ given a negative F_2 indicates that S changes from negative infinite to positive infinite.

We then plot S as a function of w/L under different μ/K (Fig. 7). For all the μ/K values, the slope S starts with 0.5 when the column is extremely slender ($w/L \ll 1$), which agrees with the prediction of Euler's elastica. For an almost incompressible material with $\mu/K = 0.005$, as the column becomes thicker (w/L increases), the slope S decreases but remains positive until $w/L = 0.103$, at which the buckling mode transitions from continuous to snapping-through. The sign of S flips again at $w/L = 0.238$ from negative to positive, indicating the transition of the buckling mode from snapping-through to snapping-back. This critical $w/L = 0.238$ perfectly matches our previous numerical result [19]. When μ/K is larger, corresponding to a more compressible material, the sign of S also flips twice, but the critical w/L for the transitions of buckling modes increase.

To thoroughly investigate the effect of shear-to-bulk modulus ratio μ/K on the transitions of buckling modes, we plot a phase diagram (Fig. 8a) to demarcate the boundaries between the three buckling

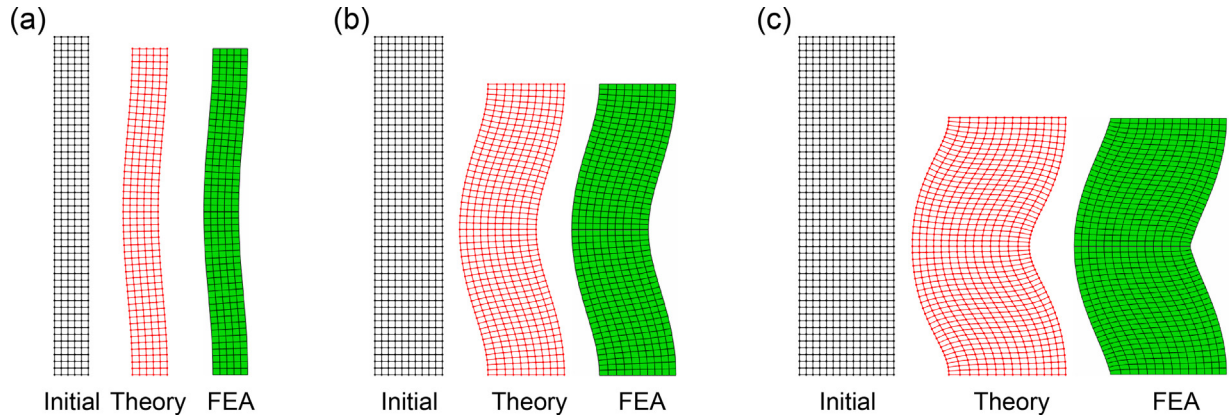

Fig. 5. Comparison of the buckled shapes in the asymptotic analysis and FEA under $\mu/K = 0.005$ for the three column buckling modes: (a) continuous ($w/L = 0.10$), (b) snapping-through ($w/L = 0.20$), and (c) snapping-back ($w/L = 0.28$). The black lattices denote the initial shapes, whereas the red and green lattices denote the buckled shapes predicted by the asymptotic analysis and FEA, respectively, under a strain ε 5% higher (continuous and snapping-through) or lower (snapping-back) than the critical strain ε_{cr}.. (For interpretation of the references to color in this figure legend, the reader is referred to the web version of this article.)

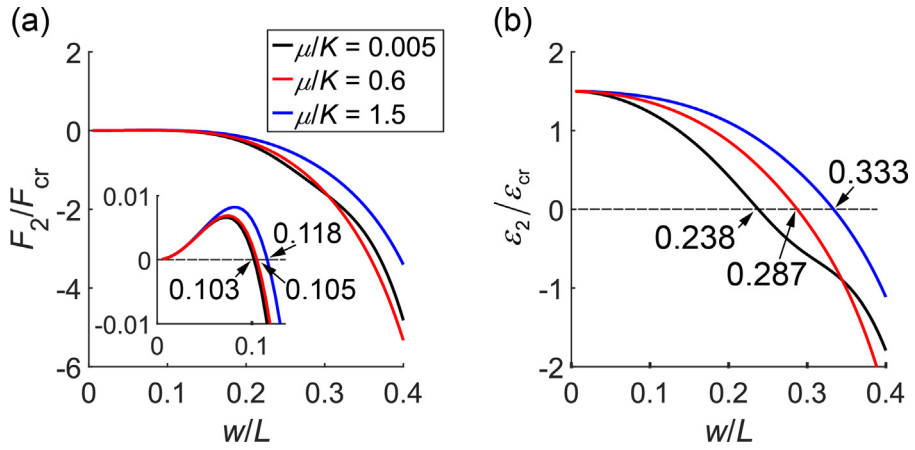

Fig. 6. Normalized second-order terms in the asymptotic expansions of (a) the compressive force F and (b) compressive strain ε as a function of the width-to-length ratio w/L under different shear-to-bulk modulus ratios μ/K. The inset of (a) magnifies the region where the force changes from positive to negative. (For interpretation of the references to color in this figure legend, the reader is referred to the web version of this article.)

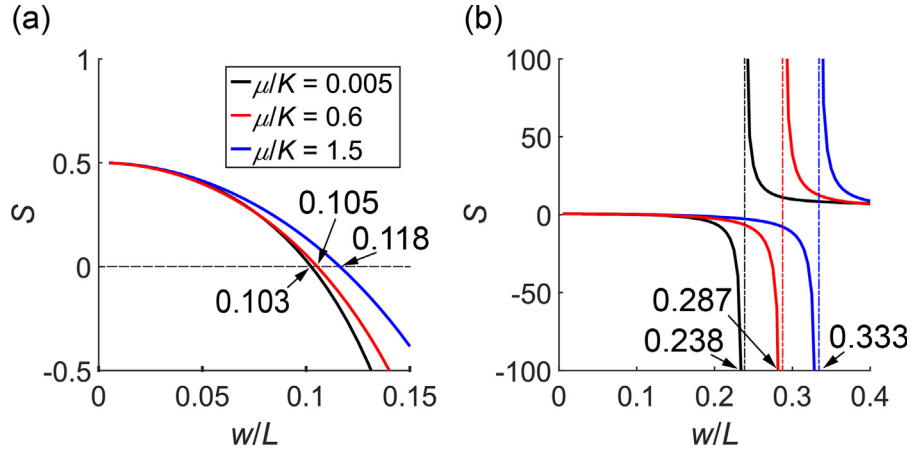

Fig. 7. Post-buckling slope S as a function of the width-to-length ratio w/L under different shear-to-bulk modulus ratios μ/K. (a) is a zoom-in view of (b) in the region where S changes from positive to negative. (For interpretation of the references to color in this figure legend, the reader is referred to the web version of this article.)

modes in the w/L-μ/K space. It is found that μ/K can significantly postpone the transition between snapping-through and snapping-back to a higher w/L, whereas the transition between continuous and snapping-through is much less affected by μ/K. This increasingly strong influence of μ/K on the post-buckling paths as w/L increases can be seen more clearly in Fig. 8b–d, in which the slopes of the $F/w\mu$-ε curves in the post-buckling regime under different μ/K are nearly equal under a low

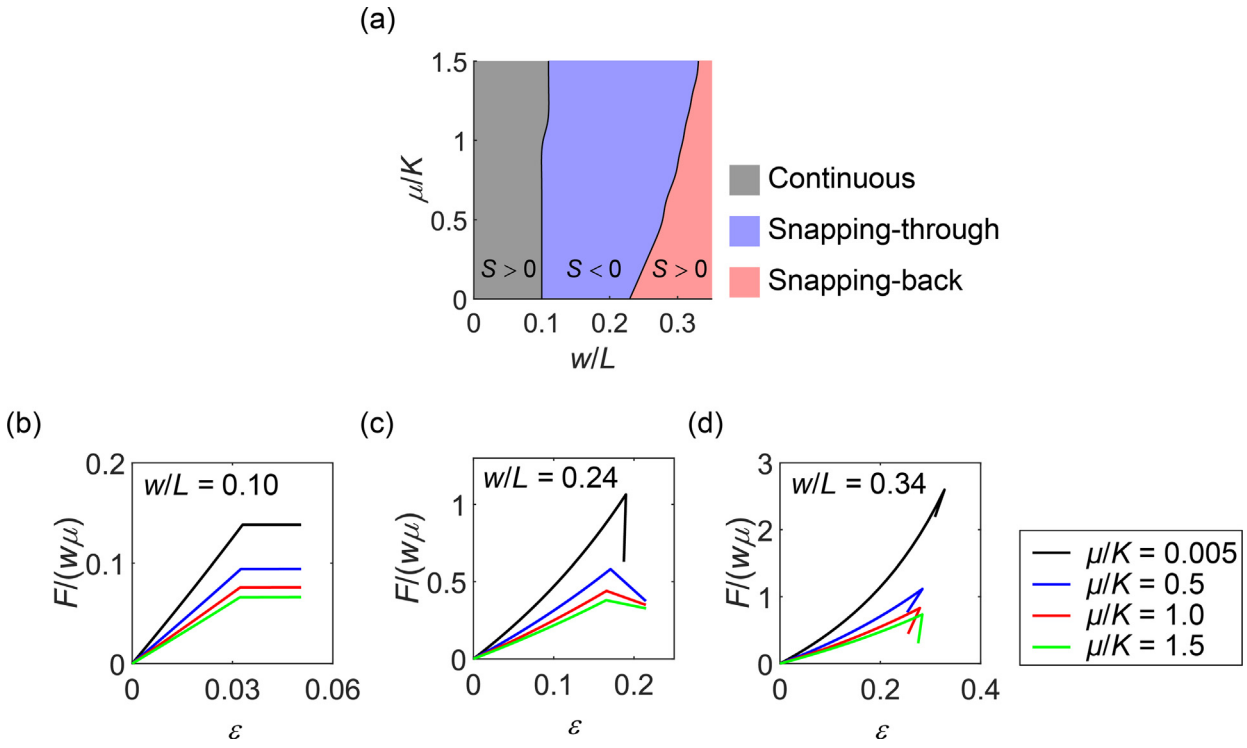

Fig. 8. Effect of the shear-to-bulk modulus ratio μ/K on the transitions of buckling modes. (a) Phase diagram of the buckling modes with respect to the shear-to-bulk modulus ratio μ/K and width-to-length ratio w/L. The black solid lines denote the boundaries between the buckling modes. (b–d) Normalized force–strain $F/w\mu$-ε curves under different μ/K from the asymptotic analysis when (b) $w/L = 0.10$, (c) $w/L = 0.24$ and (d) $w/L = 0.34$. (For interpretation of the references to color in this figure legend, the reader is referred to the web version of this article.)

w/L (Fig. 8b), whereas they differ markedly from each other under a high w/L (Fig. 8c–d).

4. Conclusion

Buckling of straight columns under axial compression has been extensively studied for centuries. Although the buckling behavior of slender columns are well predicted, the post-buckling response of wide columns with high width-to-length ratios, where material and geometric nonlinearities become crucial, remains largely unexplored. In this paper, we analytically show that for a straight hyperelastic column, the increase of its width-to-length ratio can fundamentally alter its buckling mode, from continuous to snapping-through, and to snapping-back. Correspondingly, the initial post-buckling slope flips its sign from positive to negative, and eventually back to positive. By applying a continuum mechanics-based asymptotic analysis, we determine the initial post-buckling slope as a function of the width-to-length ratio, and then identify the critical width-to-length ratios for the transitions of the buckling modes, which perfectly match the FEA results. Furthermore, we find that as the shear-to-bulk modulus ratio, which represents the material compressibility, increases, the transition between snapping-through and snapping-back buckling is postponed to a higher critical width-to-length ratio. A phase diagram of the buckling modes with respect to the width-to-length ratio and shear-to-bulk modulus ratio is constructed. Although our analysis is based on a specific neo-Hookean material model (Eq. (1)), other forms of neo-Hookean models yield similar results. The framework proposed in this paper can be applied to other constitutive laws to study the effect of different material nonlinearities on post-buckling behavior. We believe that our study provides new insights into column buckling and our findings could be of benefit to the design of mechanical metamaterials that rely on column buckling for their functionalities.

CRediT authorship contribution statement

Yuzhen Chen: Conceptualization, Methodology, Software, Writing - original draft. **Lihua Jin:** Conceptualization, Methodology, Validation, Supervision, Writing - review & editing, Funding acquisition.

Declaration of competing interest

The authors declare that they have no known competing financial interests or personal relationships that could have appeared to influence the work reported in this paper.

Acknowledgments

This work is supported by the startup fund from Henry Samueli School of Engineering and Applied Science at the University of California, Los Angeles, and Hellman fellowship [Award number 55843].

References

[1] K. Bertoldi, V. Vitelli, J. Christensen, M. Van Hecke, Flexible mechanical metamaterials, Nat. Rev. Mater. 2 (2017) 1–11, http://dx.doi.org/10.1038/natrevmats.2017.66.

[2] K. Bertoldi, P.M. Reis, S. Willshaw, T. Mullin, Negative Poisson's ratio behavior induced by an elastic instability, Adv. Mater. 22 (2010) 361–366, http://dx.doi.org/10.1002/adma.200901956.

[3] B. Florijn, C. Coulais, M. van Hecke, Programmable mechanical metamaterials, Phys. Rev. Lett. 113 (2014) 175503, http://dx.doi.org/10.1103/PhysRevLett.113.175503.

[4] H. Qiu, Y. Li, T.F. Guo, X. Guo, S. Tang, Deformation and pattern transformation of porous soft solids under biaxial loading: Experiments and simulations, Extreme Mech. Lett. 20 (2018) 81–90, http://dx.doi.org/10.1016/j.eml.2018.01.008.

[5] C. Yuan, X. Mu, C.K. Dunn, J. Haidar, T. Wang, H. Jerry Qi, Thermomechanically triggered two-stage pattern switching of 2D lattices for adaptive structures, Adv. Funct. Mater. 28 (2018) 1–9, http://dx.doi.org/10.1002/adfm.201705727.

[6] D. Yang, L. Jin, R.V. Martinez, K. Bertoldi, G.M. Whitesides, Z. Suo, Phase-transforming and switchable metamaterials, Extreme Mech. Lett. 6 (2016) 1–9, http://dx.doi.org/10.1016/j.eml.2015.11.004.
[7] J.T.B. Overvelde, S. Shan, K. Bertoldi, Compaction through buckling in 2D periodic, soft and porous structures: Effect of pore shape, Adv. Mater. 24 (2012) 2337–2342, http://dx.doi.org/10.1002/adma.201104395.
[8] C. Coulais, E. Teomy, K. De Reus, Y. Shokef, M. Van Hecke, Combinatorial design of textured mechanical metamaterials, Nature 535 (2016) 529–532, http://dx.doi.org/10.1038/nature18960.
[9] C. Coulais, A. Sabbadini, F. Vink, M. van Hecke, Multi-step self-guided pathways for shape-changing metamaterials, Nature 561 (2018) 512–515, http://dx.doi.org/10.1038/s41586-018-0541-0.
[10] J. Shim, C. Perdigou, E.R. Chen, K. Bertoldi, P.M. Reis, Buckling-induced encapsulation of structured elastic shells under pressure, Proc. Natl. Acad. Sci. USA 109 (2012) 5978–5983, http://dx.doi.org/10.1073/pnas.1115674109.
[11] P. Celli, C. McMahan, B. Ramirez, A. Bauhofer, C. Naify, D. Hofmann, B. Audoly, C. Daraio, Shape-morphing architected sheets with non-periodic cut patterns, Soft Matter 14 (2018) 9744–9749, http://dx.doi.org/10.1039/c8sm02082e.
[12] J.W. Boley, W.M. Van Rees, C. Lissandrello, M.N. Horenstein, R.L. Truby, A. Kotikian, J.A. Lewis, L. Mahadevan, Shape-shifting structured lattices via multimaterial 4D printing, Proc. Natl. Acad. Sci. USA 116 (2019) 20856–20862, http://dx.doi.org/10.1073/pnas.1908806116.
[13] T. Mullin, S. Deschanel, K. Bertoldi, M.C. Boyce, Pattern transformation triggered by deformation, Phys. Rev. Lett. 99 (2007) 84301, http://dx.doi.org/10.1103/PhysRevLett.99.084301.
[14] A. Rafsanjani, A. Akbarzadeh, D. Pasini, Snapping mechanical metamaterials under tension, Adv. Mater. 27 (2015) 5931–5935, http://dx.doi.org/10.1002/adma.201502809.
[15] D. Restrepo, N.D. Mankame, P.D. Zavattieri, Phase transforming cellular materials, Extreme Mech. Lett. 4 (2015) 52–60, http://dx.doi.org/10.1016/j.eml.2015.08.001.
[16] S. Shan, S.H. Kang, J.R. Raney, P. Wang, L. Fang, F. Candido, J.A. Lewis, K. Bertoldi, Multistable architected materials for trapping elastic strain energy, Adv. Mater. 27 (2015) 4296–4301, http://dx.doi.org/10.1002/adma.201501708.
[17] A.M.A. Van der Heijden, WT Koiter's Elastic Stability of Solids and Structures, Cambridge University Press, Cambridge, UK, 2008.
[18] C. Coulais, J.T.B. Overvelde, L.A. Lubbers, K. Bertoldi, M. van Hecke, Discontinuous buckling of wide beams and metabeams, Phys. Rev. Lett. 115 (2015) 44301, http://dx.doi.org/10.1103/PhysRevLett.115.044301.
[19] Y. Chen, L. Jin, Snapping-back buckling of wide hyperelastic columns, Extreme Mech. Lett. 34 (2019) 100600, http://dx.doi.org/10.1016/j.eml.2019.100600.
[20] E. Reissner, On one-dimensional large-displacement finite-strain beam theory, Stud. Appl. Math. 52 (1973) 87–95, http://dx.doi.org/10.1002/sapm197352287.
[21] G. Yoshiaki, Y. Tomoo, O. Makoto, Elliptic integral solutions of plane elastica with axial and shear deformations, Int. J. Solids Struct. 26 (1990) 375–390, http://dx.doi.org/10.1016/0020-7683(90)90063-2.
[22] A. Humer, Exact solutions for the buckling and postbuckling of shear-deformable beams, Acta Mech. 224 (2013) 1493–1525, http://dx.doi.org/10.1007/s00707-013-0818-1.
[23] H. Irschik, J. Gerstmayr, A continuum mechanics based derivation of Reissner's large-displacement finite-strain beam theory: The case of plane deformations of originally straight Bernoulli–Euler beams, Acta Mech. 206 (2009) 1–21, http://dx.doi.org/10.1007/s00707-008-0085-8.
[24] L.A. Lubbers, M. van Hecke, C. Coulais, A nonlinear beam model to describe the postbuckling of wide neo-Hookean beams, J. Mech. Phys. Solids 106 (2017) 191–206, http://dx.doi.org/10.1016/j.jmps.2017.06.001.
[25] S.P. Timoshenko, J.M. Gere, Theory of Elastic Stability, Courier Corporation, 2009.
[26] M.A. Biot, Exact theory of buckling of a thick slab, Appl. Sci. Res. Sect. A. 12 (1963) 183–198, http://dx.doi.org/10.1007/BF03184639.
[27] M. Levinson, Stability of a compressed neo-hookean rectangular parallelepiped, J. Mech. Phys. Solids 16 (1968) 403–415.
[28] K.N. Sawyers, R.S. Rivlin, Bifurcation conditions for a thick elastic plate under thrust, Int. J. Solids Struct. 10 (1974) 483–501, http://dx.doi.org/10.1016/0020-7683(74)90054-7.
[29] N.J.B. Young, Bifurcation phenomena in the plane compression test, J. Mech. Phys. Solids 24 (1976) 77–91, http://dx.doi.org/10.1016/0022-5096(76)90019-3.
[30] R.W. Ogden, D.G. Roxburgh, The effect of pre-stress on the vibration and stability of elastic plates, Internat. J. Engrg. Sci. 31 (1993) 1611–1639, http://dx.doi.org/10.1016/0020-7225(93)90079-A.
[31] D.G. Roxburgh, R.W. Ogden, Stability and vibration of pre-stressed compressible elastic plates, Internat. J. Engrg. Sci. 32 (1994) 427–454, http://dx.doi.org/10.1016/0020-7225(94)90133-3.
[32] Y. Cao, J.W. Hutchinson, From wrinkles to creases in elastomers: The instability and imperfection-sensitivity of wrinkling, Proc. R. Soc. A 468 (2012) 94–115, http://dx.doi.org/10.1098/rspa.2011.0384.
[33] H.H. Dai, Y. Wang, F.F. Wang, Primary and secondary bifurcations of a compressible hyperelastic layer: Asymptotic model equations and solutions, Int. J. Non-Linear Mech. 52 (2013) 58–72, http://dx.doi.org/10.1016/j.ijnonlinmec.2013.01.019.
[34] H.-H. Dai, F.-F. Wang, J. Wang, J. Xu, Pitchfork and octopus bifurcations in a hyperelastic tube subjected to compression: Analytical post-bifurcation solutions and imperfection sensitivity, Math. Mech. Solids 20 (2015) 25–52.
[35] A.A. Almet, H.M. Byrne, P.K. Maini, D.E. Moulton, Post-buckling behaviour of a growing elastic rod, J. Math. Biol. 78 (2019) 777–814, http://dx.doi.org/10.1007/s00285-018-1292-0.
[36] N. Triantafyllidis, W.M. Scherzinger, H.J. Huang, Post-bifurcation equilibria in the plane-strain test of a hyperelastic rectangular block, Int. J. Solids Struct. 44 (2007) 3700–3719, http://dx.doi.org/10.1016/j.ijsolstr.2006.10.012.
[37] A.N. Gent, I.S. Cho, Surface instabilities in compressed or bent rubber blocks, Rubber Chem. Technol. 72 (1999) 253–262, http://dx.doi.org/10.5254/1.3538798.
[38] A. Ghatak, A.L. Das, Kink instability of a highly deformable elastic cylinder, Phys. Rev. Lett. 99 (2007) 76101, http://dx.doi.org/10.1103/PhysRevLett.99.076101.
[39] E. Hohlfeld, L. Mahadevan, Unfolding the sulcus, Phys. Rev. Lett. 106 (2011) 105702, http://dx.doi.org/10.1103/PhysRevLett.106.105702.
[40] W. Hong, X. Zhao, Z. Suo, Formation of creases on the surfaces of elastomers and gels, Appl. Phys. Lett. 95 (2009) 2007–2010, http://dx.doi.org/10.1063/1.3211917.
[41] Z.P. Bažant, L. Cedolin, Stability of Structures: Elastic, Inelastic, Fracture and Damage Theories, World Scientific, Singapore, 2010.
[42] J.W. Hutchinson, Buckling and initial postbuckling behavior of oval cylindrical shells under axial compression, J. Appl. Mech. Trans. ASME 35 (1964) 66–72, http://dx.doi.org/10.1115/1.3601175.
[43] B. Budiansky, Theory of buckling and post-buckling behavior of elastic structures, Adv. Appl. Mech. 14 (1974) 1–65, http://dx.doi.org/10.1016/S0065-2156(08)70030-9.
[44] W. Hong, F. Gao, Crease instability on the surface of a solid, in: X. Chen (Ed.), Mech. Self-Assembly Sci. Appl., Springer Science & Business Media, New York, 2012, pp. 111–130.